View metadata, citation and similar papers at core.ac.uk

brought to you by CORE

provided by Juelich Shared Electronic Resources

John von Neumann Institute for Computing

Random-Lattice Simulations of Biomembranes

Ole G. Mouritsen, Myer Bloom, John H. Ipsen, Ling Miao,
Morten Nielsen, James Polson, Jenifer Thewalt,
Ilpo Vattulainen, Hong Zhu, Martin J. Zuckermann

published in

Computational Soft Matter: From Synthetic Polymers to Proteins, Lecture Notes,
Norbert Attig, Kurt Binder, Helmut Grubmüller, Kurt Kremer (Eds.),
John von Neumann Institute for Computing, Jülich,
NIC Series, Vol. **23***, ISBN 3-00-012641-4, pp. 347-374, 2004.*

© 2004 by John von Neumann Institute for Computing
Permission to make digital or hard copies of portions of this work for personal or classroom use is granted provided that the copies are not made or distributed for profit or commercial advantage and that copies bear this notice and the full citation on the first page. To copy otherwise requires prior specific permission by the publisher mentioned above.

http://www.fz-juelich.de/nic-series/volume23

Random-Lattice Simulations of Biomembranes

Ole G. Mouritsen[1], Myer Bloom[2], John H. Ipsen[3], Ling Miao[1], Morten Nielsen[4], James Polson[5], Jenifer Thewalt[6], Ilpo Vattulainen[7] Hong Zhu[4], and Martin J. Zuckermann[4,6]

[1] MEMPHYS Center for Biomembrane Physics, Physics Department, University of Southern Denmark, DK-5230 Odense M, Denmark
E-mail: ogm@memphys.sdu.dk

[2] Department of Physics and Astronomy, University of British Columbia, Vancouver, BC Canada

[3] MEMPHYS, Center for Biomembrane Physics, Department of Chemistry, University of Southern Denmark, DK-5230 Odense M, Denmark

[4] Centre for the Physics of Materials, Department of Physics, McGill University, Montreal, QC, Canada

[5] Department of Physics, University of Prince Edward Island, Charlottetown, PE, Canada

[6] Department of Physics, Simon Fraser University, Burnaby, BC, Canada

[7] Laboratory of Physics and Helsinki Institute of Physics, Helsinki University of Technology, P.O.Box 1100, FIN-02015 HUT, Finland

Lipid bilayers are models of biological membranes. The bilayers undergo thermally driven phase transitions between solid and liquid phases of different liquid-crystalline character. Cholesterol is known as a molecule that strongly modulate the phase behavior of lipid bilayers. It is surmised that the molecular evolution of sterol molecules into cholesterol was subject to a selection pressure that led to optimization of certain membrane physical properties. In this set of lecture notes we demonstrate how a combination of experiments and computer-simulation calculations can shed some light on this question by assessing the differential effects on lipid-bilayer behavior of cholesterol and one of its evolutionary predecessors, lanosterol. The simulations are based on a microscopic model for the lipid-sterol binary mixtures that consists of three basic ingredients: a representation of the translational degrees of freedom, a description of molecular conformational degrees of freedom and an expression for the potential which provides a minimal model of the interactions between the molecules. The simulations are performed using a random-lattice representation and algorithm. The methods of analysis involve umbrella sampling, histogram techniques, and finite-size scaling analysis. Results are presented for phase diagrams, order parameters, structure factors, as well as lateral diffusion. It is concluded that cholesterol in lipid membranes, in contract to lanosterol, lead to the stabilization of a particular membrane phase, the so-called liquid-ordered phase, which may present some biological advantages over more disordered liquid phases. In particular the liquid-ordered phase sustains the formation of locally ordered domains (or 'rafts') which biologists currently believes are the platform for a number of important biological functions.

1 Introduction[1]

The traditional view of biological membrane organization is that the lipid molecules form a featureless two-dimensional fluid in which proteins are kept in place by hydrophobic

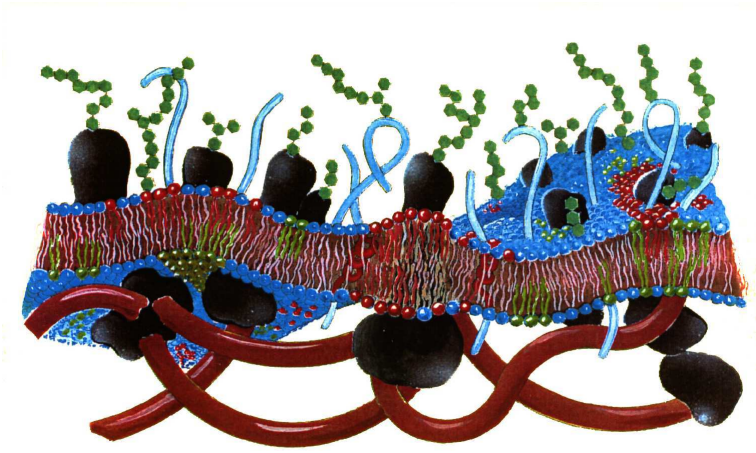

Figure 1. Schematic model of the plasma membrane of a eukaryotic cell which highlights the membrane as a composite of a central lipid bilayer sandwiched between the carbohydrate glycocalyx (which consist of polysaccharides) on the outside and the rubber-like cytoskeleton (which is a polymeric protein network) on the inside. Intercalated in the lipid bilayer are shown various integral proteins and poly-peptides. The membrane displays undulations and the lipid bilayer displays lateral heterogeneity, lipid domain formation, and thickness variations close to the integral proteins. Whereas the lipid molecules in this representation are given with some structural details, the membrane-associated proteins remain fairly featureless. In order to capture many different features in the same illustration, the different membrane components are not drawn to scale.

interactions with the lipid acyl (fatty acid) chains, hydrophilic interactions with the lipid polar heads, and perhaps anchoring interactions with the cytoskeleton[2]. In the absence of anchoring, the proteins can diffuse laterally in the plane of the membrane. A schematic illustration of of a eucaryotic cell plasma membrane is given in Fig. 1.

A large number of experimental studies of membranes and lipid bilayers have in the last decade made it increasing clear, that membranes are highly structured fluids with a substantial degree of lateral structure[3]. The advent of the so-called raft hypothesis for vertebrate and fungal plasma membranes has shaped this view[4,5]. Research into the properties of detergent resistant membrane fractions has led to the result that sorting of membrane proteins and signal transduction require co-localization of the related proteins in domains of length scale 70-200 nm, which are called rafts. The lipid compositions of these domains are far from featureless, rich in sphingolipids, cholesterol (vertebrates), or ergosterol (fungi). Moreover, the sterol is vital as its absence impedes raft formation. Finally, it has been conjectured that, in most cases, rafts form a more compact phase than that of the surrounding lipid environment, while still remaining fluid. Thus, the research on rafts suggests strongly the active roles of lipids, especially sterols, in biological functions of cells.

Since cholesterol (or ergosterol) is a key component of all plasma membranes and furthermore is central for the raft hypothesis, it is of interest to investigate, in a simple and transparent setting, the way cholesterol modulates the physical properties of lipid membranes. In particular, it is relevant to study the effect on the membrane phase equilibria and how cholesterol may induce various ordering phenomena in membranes, especially on small length scales. This calls for specific experiments on well-defined model sys-

tems together with theoretical calculations on simple molecular models. In the present set of lecture notes we shall describe a two-pronged approach to the problem by combining experiments with simulations. The experimental data is obtained mostly from nuclear magnetic resonance (NMR) spectroscopy. On the theoretical side it would be ideal to carry out Molecular Dynamics (MD) simulations on realistic atomic-scale models. Despite the advances in computer technology it it at the moment only possible to perform MD simulations on fairly small systems[6–12] (up to about 10^5 atoms, corresponding to some hundred lipid molecules and tens of thousands of water molecules) of lipid bilayers in water, possible with a single large protein or a few smaller proteins imbedded in the membrane. The MD simulations are usually limited in time up to about 10-100 ns. In the case of lipid membranes containing sterols[10,13,14] this implies that MD simulations are currently unable to investigate lipid membrane phase transitions and phase equilibria, whereas these techniques are capable of obtaining detailed information on the effect of local ordering due to different kinds of sterols. Therefore simpler coarse-gained models are called for that allow larger systems to be simulated. This is the strategy which forms the basis of the present set of lecture notes.

1.1 Lipid Bilayers are Model Membranes

It is generally difficult to investigate the properties of biological membranes at a molecular level because of the enormous chemical diversity of lipids and proteins involved. Many experimental and theoretical studies are therefore, performed on model membranes, which are composed of a few lipid and/or protein species. Most of such model membranes can be easily produced in-vitro as a result of the self-assembly process of their molecular components dispersed in aqueous media[15].

Despite of their relative chemical simplicity the model membranes exhibit sufficient complexity to mimic some of the physical characteristics of biological membranes. For example, ternary mixtures of two lipid species with cholesterol have been used by many researches as model systems for studying raft formation[4]. In these model membranes, domains where one of the lipid species forms a compact physical phase – known as the liquid ordered (**lo**) phase[16] – together with a large concentration of cholesterol molecules appear within a less compact background fluid formed by the other lipid component with very little cholesterol. The nature of the background phase is typical of single-component lipid bilayers in the liquid crystalline phase, also known as the liquid disordered (**ld**) phase[16]. We will give a description of the phases below.

We shall be particularly interested in investigating the thermodynamic phase behaviour of such model membranes with the view to understand the essential microscopic interactions underlying the phase behaviour. Our approach has been to carry out theoretical studies based on computer simulations of microscopic interaction models in parallel with experimental investigations. The microscopic interaction models that our group has used or developed during the past two decades have varied focuses, depending on the specific physical questions under investigation[17,18]. Our earlier work involved the use of lattice models[16,18,19]. Our more recent investigations, however, focused on the development and study of off-lattice models that are able to provide a genuine description of the fluid characteristics of both the **ld** and the **lo** phases[20]. In the present lecture notes, we present our work on the application of off-lattice models to the physical properties of lipid-sterol bilayers[21,22].

The methodological backbone of our computer simulations is the Metropolis Monte Carlo (MC) method. This method guarantees that a simulated system will reach its state of thermodynamic equilibrium. A tutorial on the use MC methods for the simulation of lattice and off-lattice models for lipid bilayers and lateral organization has appeared recently[23] as well as a general review on lattice models used for simulation of membranes interacting with proteins, peptides, sterols, drugs, and other solutes[19]. The present lecture notes will furnish a description of the use of the method together with many other simulational techniques within the specific context of our modeling.

It is important to note at the outset that, given the available computational capacity, our simulations are limited in terms of the size of the sample, which is restricted to systems of the order of 10^4 lipid chains for our lattice models and 10^3 lipid chains for the off-lattice models. This enables us to study the nature of distinct phases and phase transitions using dedicated techniques, but not systems with a distribution of domains of the sizes predicted for rafts.

1.2 Pure Lipid Bilayers

Our approach has been to study model systems with the least number of molecular components first and then proceed to systems of several components[17,18,20]. The initial systems are pure, single-component lipid bilayers which themselves exhibit several phase transitions. We will concentrate on one particular phase transition known as the main phase transition, which gives much insight into the interactions between lipid molecules. The transition takes the bilayer from the gel phase to the liquid crystalline phase as the temperature is increased and is abrupt, highly entropic. The gel phase is a two-dimensional (2d) crystalline phase in which conformationally ordered lipid chains form a structural lattice. Here conformationally ordered lipid chains are almost fully extended with very few gauche bonds towards their free ends. To describe the nature of the gel phase in more detail, we have renamed it the solid-ordered (**so**) phase. In contrast the liquid crystalline phase is a fluid phase in which conformationally disordered lipid chains can diffuse laterally in the bilayer plane. Here the conformationally disordered lipid chains contain many gauche bonds, leading to a reduced apparent length, but an increased cross-sectional area. The quantitative properties of the main phase transition depend both on the intrinsic chain length and unsaturation and on the type of polar head of the lipid molecule involved as well as on the ionic character of the aqueous medium hydrating the polar heads.

1.3 The Liquid-Ordered Phase and Sterol Evolution

The concept of liquid-ordered (**lo**) phase emerged already 15 years ago from both experimental and theoretical studies of the phase behaviour of dipalmitoyl phosphotidylcholine (DPPC)-cholesterol bilayers[16]. DPPC is a glycerophospholipid with a zwitterionic polar head and two saturated (16:0) acyl chains and appears as a molecular component of many biological membranes. The experimental phase diagram of DPPC-cholesterol multibilayer liposomes was first deduced by Vist and Davis[24] from both deuterium nuclear magnetic resonance (^{2}H-NMR) and differential scanning calorimetry (DSC) data. The same topology was found for the phase diagram of PPetPC-cholesterol bilayers[22] as shown in Fig. 2a, even though PPetPC differs in structure from DPPC in that one *trans*–double bond

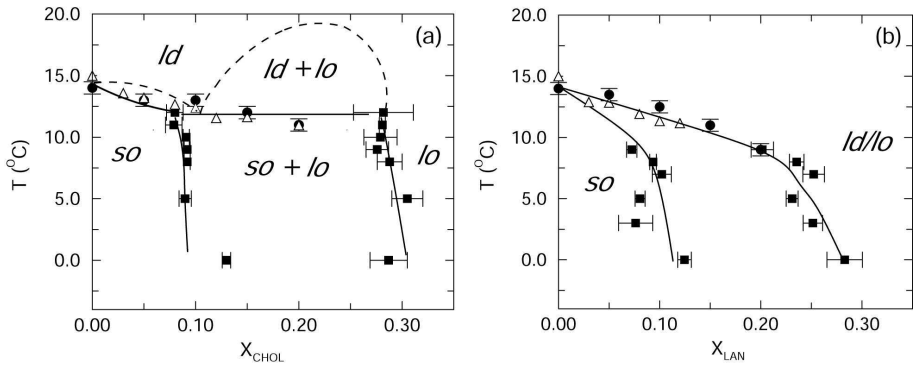

Figure 2. Experimental phase diagrams as determined by differential-scanning calorimetry (open triangles) and by NMR spectroscopy (solid squares and solid circles). (a) PPetPC-cholesterol systems; (b) PPetPC-lanosterol systems. The lines connecting the points are guides to the eyes. The phase boundaries indicated by the dashed lines in (a) are not derived from any experimental data and are shown only to illustrate the qualitative structure of the phase diagram, which is consistent with the thermodynamic phase rules.

replaces a single C–C bond in DPPC at carbon seven. Qualitatively similar phase diagrams were also found by Thewalt et. al.[25] for several other systems of binary mixtures containing cholesterol and lipids with PC polar heads. The most important feature of these phase diagrams is that an abrupt main phase transition is absent for cholesterol concentrations greater than 20-30 mol%, and a new phase appears in this region of the phase diagrams. This new phase is a fluid phase where the lipid chains are reasonably ordered conformationally as demonstrated by the ^{2}H-NMR data. Vist and Davis[24], who first identified this new phase named it the β phase. In the first theory for the experimental phase diagram, Ipsen et al.[16] renamed this phase the liquid-ordered or **lo** phase since this phase is a compact liquid phase with conformationally ordered chains[16]. This concept has gained a prominent position in raft research, because several experimental studies on rafts suggest that rafts have the physical characteristics of the **lo** phase[4,5]. It is worth pointing out that the only **lo/ld** phase separation observed for single lipid-cholesterol bilayers occurs close to the melting temperature of the pure lipid system. Thus it is reasonable to assume that mixtures of lipids and cholesterol would require at least some high-$T_{\rm m}$ components in order to display the **lo** phase at body temperature.

Given the existing understanding of the equilibrium phase behaviour of the single lipid-cholesterol bilayers and the underlying microscopics and inspired by the work of Bloch on sterol evolution[26] we have recently carried out a comparative study of lipid-cholesterol and lipid-lanosterol bilayers, both experimentally and theoretically by computer simulations. Lanosterol is the first cyclic precursor of cholesterol in the biosynthetic pathway and is regarded as a molecular fossil by Konrad Bloch who proposed that the evolutionary sequence for cholesterol is preserved in its biosynthetic pathway[26].

The differences in the phase behaviour of the two types of lipid-sterol systems are illustrated in the two phase diagrams in Fig. 2[22]. The phase diagram in Fig. 2a shows that the **lo** phase is a well defined thermodynamic phase distinctly separate from the **ld** phase, but that it can coexist with the **ld** phase under appropriate temperatures and concentrations. In contrast the phase diagram in Fig. 2b shows that for PPetPC-lanosterol multi-bilayer

systems the **lo** and the **ld** phases are no longer thermodynamically distinct, i.e. that the coexistence of the two phases is absent.

Moreover, our experimental data for PPetPC-lanosterol and PPetPC-cholesterol show that cholesterol induces greater conformational order in PPetPC-lipid chains than lanosterol[22]. It may be reasonable to expect such a relative effect also to apply to DPPC-cholesterol and DPPC-lanosterol bilayers. Hence a possible hypothesis is that one reason for the evolutionary optimization of cholesterol is that it is able to induce the formation of rafts better than lanosterol. There is in fact some evidence that lanosterol cannot induce raft formation[27].

2 Off-Lattice Models[20–22,29]

The first step in a statistical mechanical study of a model membrane system is to construct a model describing the microscopic physics of the membrane. The model should contain two basic ingredients: 1) a specific description of the microscopic states of the membrane, i.e., the relevant microscopic degrees of freedom; 2) a specific expression of the total interaction potential energy of the system as a function of the relevant degrees of freedom. In both parts, approximations or simplifications are necessary, mainly due to the limited computational capacity available and the need to underline among the almost formidably complicated microscopic details the general mechanisms that are essential to the macroscopic phenomena under investigation. The models to be described below may in fact be called 'minimal' in terms of the approximations and simplifications involved.

The basic molecular degrees of freedom of a lipid-bilayer membrane consists of both the positional (molecular center of mass) and internal (conformational) degrees of freedom, and both types are relevant to the phase behaviour of the membrane. The description of the positional degrees of freedom is straightforward, given by specifying the spatial coordinates of the molecules. Our description of the conformational isomerism of the lipid chains is a minimal one. Only two internal states are used to approximate the very large spectrum of conformations possible for a phospholipid chain: One state, the 'ordered' state, has zero internal energy and is non-degenerate, characteristic of the conformational state of a lipid chain in the gel or **so** phase. The other state, the 'disordered' state, is characteristic of the average conformational state of a lipid chain in the liquid-crystalline or **ld** phase. This state has a high internal energy, reflecting that energy is required for conformational excitations, and a high degeneracy, effectively representing the large number of conformational excitations of that a phospholipid chain can assume in the **ld** phase due to the presence of many gauche bonds. This idea was first proposed and used by Doniach[17]. Both cholesterol and lanosterol are rigid molecules in comparison with the phospholipid chains and we assume that they have no conformational degrees of freedom.

In constructing the function describing the interaction potential energy, several approximations have also been made. First, the interactions between the amphiphilic molecules (phospholipid, sterol) and the water molecules, which are predominantly responsible for stabilizing a bilayer membrane, are approximated by a surface-pressure parameter Π, as first suggested by Marčelja[30]. Secondly, the non-covalent interactions between the amphiphilic molecules may, to a first approximation, be considered as being pair-wise, of the Van der Waals type, and effective only over a short range of molecular length scale. Finally, only one monolayer is modeled based on the assumption that the two monolayers constitut-

ing a lipid bilayer are independent of each other. In essence, our model system consists of microscopic 'particles' – distinct lipid chains and sterol molecules – which move within a two-dimensional plane and which interact in a pairwise manner, as described below. In the rest of this text, the term 'particle' may refer either to a lipid chain or to a sterol molecule.

The total potential energy function that models molecular interactions in the lipid-sterol bilayer systems in our simulations is then given by

$$H = H_0 + H_{\mathrm{o-s}} + H_{\mathrm{d-s}} + H_{\mathrm{s-s}} \quad . \tag{1}$$

H_0 is the potential energy function describing the interactions between the phospholipid molecules, whose specific form is as follows

$$H_0 = \sum_i E_{\mathrm{d}} \mathcal{L}_{i\mathrm{d}} + \sum_{\langle i<j \rangle} V_{\mathrm{o-o}}(R_{ij}) \mathcal{L}_{i\mathrm{o}} \mathcal{L}_{j\mathrm{o}} + \sum_{\langle i<j \rangle} V_{\mathrm{o-d}}(R_{ij}) \{ \mathcal{L}_{i\mathrm{o}} \mathcal{L}_{j\mathrm{d}} + \mathcal{L}_{j\mathrm{o}} \mathcal{L}_{i\mathrm{d}} \} + \Pi \cdot A \quad . \tag{2}$$

Here i is an index labeling the 'particles' (lipid chains and sterol molecules) in the system. Correspondingly, $\mathcal{L}_{i\mathrm{o}}$ and $\mathcal{L}_{i\mathrm{d}}$ are occupation variables which are unity when the ith particle is a lipid chain in the ordered state and the disordered state, respectively, and which are zero otherwise. E_{d} is the excitation energy of the conformationally disordered state, and $V_{\mathrm{o-o}}(R)$ and $V_{\mathrm{o-d}}(R)$ are distance-dependent and chain-conformation-dependent interactions between two lipid chains. $\langle i < j \rangle$ denotes a summation over nearest neighbors, corresponding to the approximation of short-range interactions. The energy of interaction between two chains which are both in the disordered state is approximated to be zero, which sets the reference point for energy. This potential energy function, H_0, together with the configurational degeneracy of the disordered state, provides a minimal model for the main phase transition of single component bilayers.

$H_{\mathrm{o-s}}$, $H_{\mathrm{d-s}}$ and $H_{\mathrm{s-s}}$, as indicated by the various subscripts, represent the pairwise interactions between an ordered chain and a sterol molecule, a disordered chain and a sterol molecule, and two sterol molecules, respectively. They are written explicitly as follows:

$$\begin{aligned} H_{\mathrm{o-s}} &= \sum_{\langle i<j \rangle} V_{\mathrm{o-s}}(R_{ij}) \{ \mathcal{L}_{i\mathrm{o}} \mathcal{L}_{j\mathrm{s}} + \mathcal{L}_{j\mathrm{o}} \mathcal{L}_{i\mathrm{s}} \} \\ H_{\mathrm{d-s}} &= \sum_{\langle i<j \rangle} V_{\mathrm{d-s}}(R_{ij}) \{ \mathcal{L}_{i\mathrm{d}} \mathcal{L}_{j\mathrm{s}} + \mathcal{L}_{j\mathrm{d}} \mathcal{L}_{i\mathrm{s}} \} \\ H_{\mathrm{s-s}} &= \sum_{\langle i<j \rangle} V_{\mathrm{s-s}}(R_{ij}) \{ \mathcal{L}_{i\mathrm{s}} \mathcal{L}_{j\mathrm{s}} \} \quad . \end{aligned} \tag{3}$$

Again $\mathcal{L}_{i\mathrm{s}}$ is an occupation variable which is unity when the ith particle is a sterol molecule and is zero otherwise. Clearly, $\mathcal{L}_{i\mathrm{s}} + \mathcal{L}_{i\mathrm{o}} + \mathcal{L}_{i\mathrm{d}} = 1$. $V_{\mathrm{o-s}}(R)$ and $V_{\mathrm{d-s}}(R)$ are the distance-dependent, chain-conformation-dependent interaction potentials between a sterol molecule and a lipid chain. Similarly $V_{\mathrm{s-s}}(R)$ is the interaction between two sterol molecules.

All of the pair-wise interaction potentials are approximated by a sum of a hard-core repulsive potential of range d, a short-range square-well potential of range R_0, $V^{\mathrm{s}}(R)$, and a longer-range attractive square-well potential of range $l_{\max}$, $V^{\mathrm{l}}(R)$. $V^{\mathrm{s}}(R)$ and $V^{\mathrm{l}}(R)$

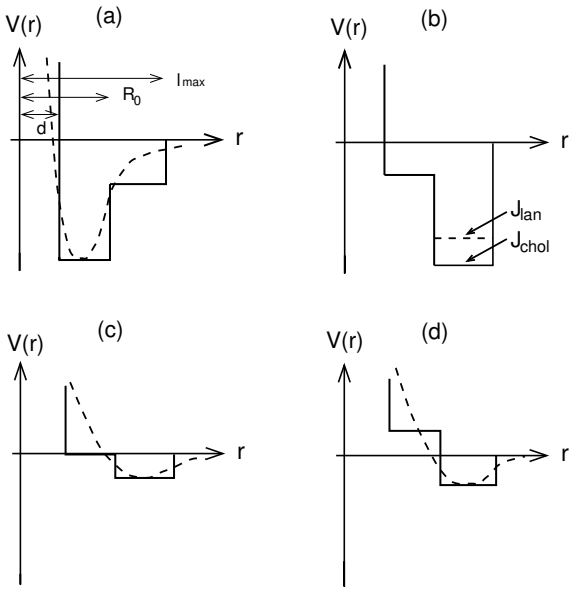

Figure 3. Schematic illustration of the model interaction potentials. (a) $V_{\mathrm{o-o}}(R)$, where subscript 'o' refers to a lipid chain in the conformationally ordered state; (b) $V_{\mathrm{o-s}}(R)$, where the depth of the potential corresponding to s= chol is represented by a solid line and a parameter J_{chol} and that corresponding to s= lan is represented by a dotted line and a parameter J_{lan}; (c) $V_{\mathrm{d-s}}(R)$, where subscript 'd' refers to a lipid chain in the disordered state; (d). $V_{\mathrm{s-s}}(R)$. d is the hard-core radius, R_0 is the range of the short-range potentials and $l_{\max}$ is the effective range of the long-range potentials. The ratio of R_0/d is chosen so that the average surface area of a sterol molecule is approximately 30% larger than that of a lipid chain in the ordered state. The dashed lines illustrate the more realistic interaction potentials that the model potentials approximate.

are given by

$$V^{\mathrm{s}}(R) = \begin{cases} -V^{\mathrm{s}} & , \quad d < R \leq R_0 \\ 0 & , \quad \text{otherwise} \, , \end{cases} \tag{4}$$

$$V^{\mathrm{l}}(R) = \begin{cases} -V^{\mathrm{l}} & , \quad d < R \leq l_{\max} \\ 0 & , \quad \text{otherwise} \, , \end{cases} \tag{5}$$

where the specific values of V^{l} and V^{s} depend on both the molecular type and the conformational state of the interacting species. Here $l_{\max}$ is a cutoff distance which will be defined when the simulation algorithm is discussed in the next subsection.

The pair-wise interaction potentials are illustrated in Fig. 3, and their construction is based on the hypothesis that cholesterol interacts with lipid molecules as follows. Cholesterol, with its streamlined, rigid hydrophobic backbone, prefers the lipid chains in its immediate neighborhood to be in the conformationally ordered (rigid) state by suppressing the formation of *gauche* bonds in those chains. At the same time cholesterol tends to disrupt laterally ordered packing of conformationally ordered chains if it is in their midst. A comparison between Fig. 3a and Fig. 3b illustrates the latter, 'crystal-breaker' mechanism, as the interactions involved imply that a cholesterol molecule dissolved in an ordered-chain

environment tends to have a larger surface area than that of a lipid chain, thereby breaking the lateral order of ordered chains. Similarly, a comparison between Fig. 3b and Fig. 3c shows that the former, 'chain-rigidifier' mechanism is modeled by a strong interaction between cholesterol and a neighboring, conformationally ordered lipid chain and a weaker interaction with a conformationally disordered lipid chain.

The values of all the relevant parameters in the model are chosen as follows. The unit of length scales in the model is for convenience set at the hard-core diameter, d, of the interaction potentials and the unit of energy is defined to be a quantity J_0. In order to convert the energy and length scales into units relevant for lipid bilayer systems, J_0 should be of the order 10^{-20}J and d of the order 5 Å. The lateral pressure, Π, is fixed at $\Pi d^2/J_0 = 3.0$. The radius of the short-range potential, Eq. (4), is set at R_0/d = 1.3. The values of Π and R_0 are chosen such that the change in surface area across the main transition is comparable to that of a pure PC (DPPC) bilayer system. The excitation energy of the disordered state of lipid chains is chosen to be $E_{\rm d} = 2.78J_0$, and the degeneracy, $D_{\rm d}$, of the disordered state, is taken to be $\ln D_{\rm d} = 12.78$. These values are the same as for the 10th state of the Pink Model for the main phase transition of single component PC bilayers with saturated chains[31] . Other parameters appearing in the definition of the interaction potentials are summarized in Table 1(a). They are chosen such that the theoretical phase diagram of the lipid-cholesterol model system is similar to that of the DPPC-cholesterol system.

(a)

	$V_{\rm o-o}$	$V_{\rm o-d}$	$V_{\rm d-d}$	$V_{\rm s-s}$	$V_{\rm s-d}$
long range	0.40	-0.15	0.20	0.20	0.00
short range	0.45	0.40	-0.20	-0.15	-0.065

(b)

	Cholesterol	Lanosterol
$V^{\rm l}_{\rm o-s}$ (J)	0.85	0.75
$V^{\rm s}_{\rm o-s}$	-0.625	-0.525

Table 1. Interaction parameters for the model potentials for the two types of lipid-sterol membranes. (a) The parameter values for the interaction potential, $V_{\rm o-o}$, between two lipid chains in the ordered state, the interaction potential, $V_{\rm o-d}$, between a lipid chain in the ordered state and a lipid chain in the disordered state, the interaction potential, $V_{\rm d-d}$, between two lipid chains in the disordered state, the interaction potential, $V_{\rm s-s}$, between two sterol molecules, and the interaction potential, $V_{\rm s-d}$, between a lipid in the disordered state and a sterol molecule. Note that these values are identical for both the lipid-cholesterol and the lipid-lanosterol systems. (b) The parameter values for the interaction potential, $V_{\rm o-s}$, between a lipid chain in the ordered state and a sterol molecule, where the subscript s corresponds to either chol or lan, respectively. All the parameters are given in units of J_0 (see text).

The parameters given in Table 1(b) reflect our – again, minimal – modeling of differences in lipid-cholesterol and lipid-lanosterol interactions. The model arises from a comparative analysis of the molecular structures of the two sterols which are shown in terms of space-filling models in Fig. 4. Figure 4 indicates that the major structural difference is on their respective α-faces. In detail, cholesterol has a smooth α-face, whereas the α-face of

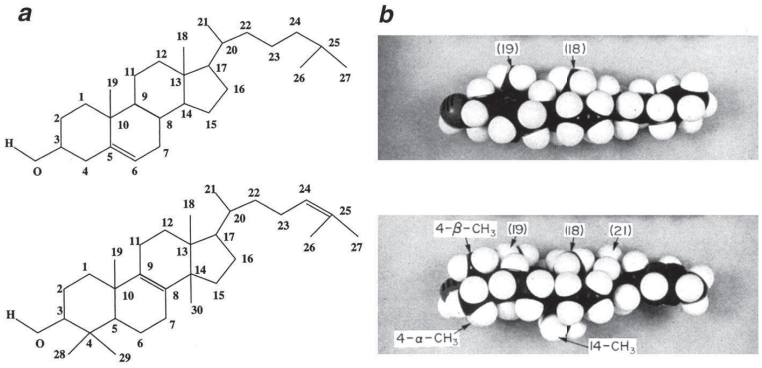

Figure 4. Molecular structures of cholesterol (top) and lanosterol (bottom). (a) Chemical structures; (b) Space-filling models. The three additional methyl groups on lanosterol are indicated in (b) as 14-CH_3, 4-α-CH_3, and 4-β-CH_3.

lanosterol has an extra methyl group, which forms a rather significant protrusion. Together with two other additional methyl groups this α-face protrusion would decrease the ability of lanosterol to order neighboring lipid chains. It is interesting to note that the α-face methyl group is the first one to be removed in the biosynthetic pathway at considerable cost in metabolic energy.

Hence, in our theoretical model, the microscopic lipid-cholesterol and lipid-lanosterol interactions differ only in the part that describes the interaction between a sterol molecule and an ordered lipid chain, $V_{\mathrm{o-s}}$. The values listed in Table 1(b) correspond to a decreased strength of the cohesive lipid-lanosterol interaction relative to that of the cohesive lipid-cholesterol interaction. They were determined by fitting the theoretically calculated value of the lipid-chain order parameter, ϕ (see later), to the acyl-chain order parameter experimentally derived from the ^{2}H-NMR data, over a significant range of sterol concentrations for both types of the lipid-sterol systems. The fitting was carried out at a single temperature, which was relatively high so that no complications associated with phase transitions arose. The fit is shown in Fig. 5.

3 Simulation Methods

3.1 Monte Carlo Techniques

In our computer simulations of the thermodynamic phase behaviour of the models described in the previous section, the MC method provides the backbone method. Generally speaking, the MC procedure in each simulation samples stochastically and ergodically the complete configuration space spanned by all possible microscopic states of the system and generates a Markovian sequence of microscopic states whose distribution over the configuration space approximates the equilibrium distribution. Explicitly, each simulation consists of many repeated cycles of procedures, and each cycle, labeled by an integer n, is implemented as follows:

1. An arbitrary microscopic state, Ω_n, is chosen.

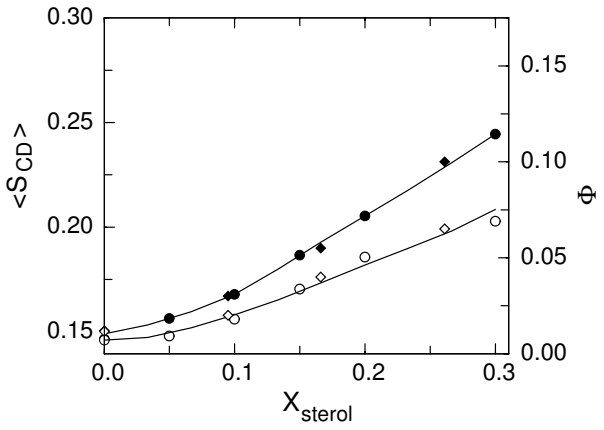

Figure 5. Fitting of the theoretical (ϕ) order parameter to the equilibrium averages of the experimental order parameter (S_{CD}, as given in Eq. (14)) which leads to the specific value of J used for lipid-lanosterol interactions in the model. The experimental data are obtained at $T = 40^{\circ}\mathrm{C}$. The theoretical data are calculated for a system containing $N = 1600$ particles at a temperature of $T = 1.0359T_{\mathrm{m}}$. Corresponding to cholesterol and lanosterol, the experimental data are shown by filled and open circles, respectively, and the theoretical data are given by filled and open diamonds, respectively. The lines connecting the points are guides to the eye.

2. Next a trial microscopic state, Ω_{t}, is established by a random, ergodic sampling of the complete configuration space.

3. A quantity, $\Delta\tilde{H} \equiv \tilde{H}(\Omega_{\mathrm{t}}) - \tilde{H}(\Omega_n)$, is calculated, where $\tilde{H}$ depends both on the potential-energy function of the system and on the choice of thermodynamic ensemble.

4. A random number, r, is generated.

5. If $r < \exp(-\Delta\tilde{H}/k_{\mathrm{B}}T)$, the trial microscopic state, Ω_{t}, is accepted as the new configuration of the system, i.e., $\Omega_{n+1} = \Omega_{\mathrm{t}}$. Otherwise the system remains in the same state, i.e., $\Omega_{n+1} = \Omega_n$.

6. Quantities of interest for ensemble averaging are calculated and recorded.

7. A new trial microstate, Ω_{t}, is chosen again randomly and ergodically, and the $n + 1$ cycle is started by going back to step 3.

It is implied in the MC procedure that a specific choice of thermodynamic ensemble has been made, which affects both the definition of the complete configuration space and the definition of $\Delta\tilde{H}$. In addition to choosing temperature T and surface pressure Π as thermodynamic control variables, we are still left with two different choices regarding the number of 'lipid-chain' particles, N_{l} and the number of 'sterol' particles, N_{s}: (a) fixing both N_{l} and N_{s}; and (b) fixing the total number of particles, $N_{\mathrm{l}} + N_{\mathrm{s}}$, and letting the chemical composition of the system fluctuate under the control of an effective chemical potential, μ_{Δ}. We take μ_{Δ} to represent the difference between the chemical potentials of the lipid and the sterol particles. We have used either (a) or (b) in our simulations,

depending on the specific questions that we have asked about the system. In the following, we will call (a) the 'canonical ensemble,' and (b) the 'semi-grand canonical ensemble.'

In simulations formulated in the canonical ensemble, $\Delta\tilde{H}$ in each MC cycle is simply given by

$$\Delta\tilde{H} = H(\Omega_{\rm t}) - H(\Omega_n) - k_{\rm B}TN\ln[A(\Omega_{\rm t})/A(\Omega_n)] \; , \tag{6}$$

where H is just the potential-energy function defined in Eq. (1). The logarithmic term arises from any possible changes in the area of the system (see later). In simulations formulated in the semi-grand canonical ensemble, however,

$$\Delta\tilde{H} = H(\Omega_{\rm t}) - H(\Omega_n) - k_{\rm B}TN\ln[A(\Omega_{\rm t})/A(\Omega_n)] + \mu_\Delta[N_{\rm l}(\Omega_{\rm t}) - N_{\rm l}(\Omega_n)] \; . \tag{7}$$

Of course, in the two ensembles, the procedures of sampling their corresponding complete configuration spaces differ also. The differences will be pointed out wherever appropriate in the following specific discussions of the sampling step 2 in the general procedure.

The sampling step 2 is a combination of different types of 'moves' which generate changes in the microscopic state of the system, that are associated with the different types of degrees of freedom. We will discuss these moves in detail below.

3.1.1 Dealing with the Translational Degrees of Freedom: An Random-Lattice Algorithm

The positions of the particles in a system form a part of the definition of a microscopic state and are essential to calculations of the potential energy arising from position-dependent interactions between the molecular constituents. In dealing with interactions that are pairwise and short-ranged, the most important information required is the local environment of each individual particle, such as the distribution of other particles in its neighborhood and their distances to it. In conventional off-lattice simulations, it is usually one of the most time-consuming steps to obtain this information from each given configuration of molecular positions. We now describe a simulational algorithm, a so-called dynamic random-lattice algorithm, which handles structural information in a manner that is distinctly different from conventional algorithms, and which at the same time achieves high computational efficiency. The algorithm assures that the system can be simulated in a fluid phase.

Our algorithm is an adapted version of the dynamic-triangulation algorithm used for modeling random surfaces. It performs two essential tasks: 1) The generation of the (sub)configuration space associated with the translational degrees of freedom; 2) The generation and the retention of a compact data structure that allows efficient access to structural information contained in each configuration of particle positions. The data structure is based on triangulation of each spatial configuration of the particles. The triangulation itself is performed as follows: an initial configuration in which the particles are positioned with their centers on a regular triangular lattice is used and each particle is linked to its six nearest neighbors by 'tethers.' The lattice configuration is then represented by a network of tethers forming triangles; the term 'triangulation' refers to this representation. The tether network can then be altered randomly, through the moves described below, to provide the subspace of microscopic states that are associated with particle positions. The interacting particle pairs are those that are connected by the tethers.

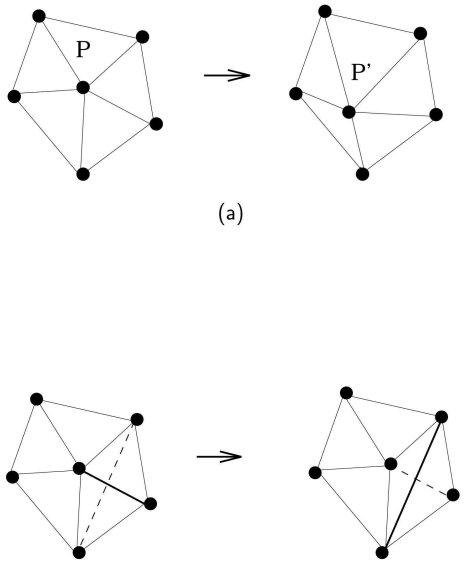

Figure 6. (a) Particle Displacement. The particle at position P is moved to position P′. (b) Link Flip. A tether (shown as a thick line) is replaced by another tether along the unoccupied diagonal (once the first tether is removed) provided that the new tether length does not exceed $l_{\max}$.

3.1.2 Particle Displacement

This move is illustrated in Fig. 6a. A particle is chosen at random and its center is subject to a random displacement $(\delta x, \delta y)$ where

$$\begin{aligned} \delta x &= (2\zeta_x - 1)\delta r_{\mathrm{MAX}} \\ \delta y &= (2\zeta_y - 1)\delta r_{\mathrm{MAX}} \quad . \end{aligned} \tag{8}$$

ζ_x and ζ_y are random numbers, $0 \leq \zeta_{x(y)} \leq 1$. The value of δr_{MAX} is adjusted during the simulations so that approximately 25 % of trials are accepted. Consistent with the hard-core repulsion between two interacting particles, moves which would result in an overlap of the hard cores of the particle are always rejected. Another constraint is that the length of every tether is not allowed to exceed a maximum value $l_{\max}$.

3.1.3 Link Flip

The second move is referred to as 'link flip,' which alters the local connectivity in the tether network. It is shown schematically in Fig. 6b. In each configuration of the tether network, each tether forms one diagonal of a quadrilateral formed by the two adjacent triangles. In the 'link flip,' a tether is chosen at random and then removed; a new tether is placed along the other diagonal of the quadrilateral, provided that its length does not exceed $l_{\max}$.

3.1.4 Change of System Size

Consistent with our choice of thermodynamic ensemble, where the surface pressure is a control parameter, fluctuations in the total area of the system must be sampled. In our simulations this is achieved via a third move: a random uniform expansion or contraction of the whole system. In this step, a random change in the size of the system is generated as

$$\delta L = (2\zeta - 1)\delta L_{\mathrm{MAX}} \tag{9}$$

where ζ is a random number, $0 \leq \zeta \leq 1$; and the coordinates of all particles in the system are rescaled accordingly. If the distance between any two particles after the rescaling is smaller than the hard-core diameter the change is always rejected. The maximum possible size change, δL_{MAX}, is adjusted during the simulation to give an acceptance ratio of about 50 %. The logarithmic term in Eq.(6) or Eq.(7) will necessarily be nonzero following this types of moves. A detailed discussion of this types of sampling moves are given in the book by Frenkel and Smith[28], pp. 116-122.

3.1.5 Dealing with the Conformational and Compositional Degrees of Freedom

In simulations in the canonical ensemble, sampling the part of the configuration space that is associated with the conformational degrees of freedom of the lipid chains is straightforward. A lipid chain is chosen at random and its conformational state is always changed in the trial state. For example, if the chain is in the ordered state, it will be in the disordered state in the trial state and vice versa.

In the case of the semi-grand canonical ensemble, a different updating procedure is used, where the conformational degrees of freedom and the compositional degrees of freedom are handled on the same footing. Explicitly, each particle in the system is assigned one of three possible 'internal' states: the conformationally ordered and disordered states of a lipid chain, or a third, 'sterol' state. Then a random number is used to choose among the three internal states now available.

In order to ensure detailed balance in the simulations, or the symmetry of the Markov chain generated by the algorithm, all of the different moves discussed above are combined in a random manner. In other words, the simulation algorithm does not impose any preferred sequential order in the sampling procedures that update different types of degrees of freedom[28]. Monte Carlo step (MCS), a time unit for the simulations, is defined to be the time needed to perform on average one complete pass through all the different types of moves.

3.2 Umbrella Sampling[28]

Up to this point, we have given a detailed recipe for performing an MC simulation for a system described by the potential-energy function of Eq. (1). We now discuss a method for determining phase boundaries specific to our study of the phase behavior of lipid-sterol bilayer membranes. This method is a version of umbrella sampling and it is particularly useful for determining phase transitions whose kinetics are strongly hysteretic. The transitions between the **so** and the **ld** phases in our systems are precisely such transitions. The high free-energy barriers separating the two coexisting phases make it very difficult to achieve an adequate sampling of both phases.

This difficulty was overcome by the use of a simulation technique, which exploits the idea of developing an 'artificial' potential-energy function that yields a considerably diminished free-energy barrier. The simulation carried out for the artificial potential-energy function is able to yield an adequate sampling of the two coexisting phases. The equilibrium distribution functions (defined below) for the original potential-energy function can then be established from simulations based on the modified potential-energy function through a simple re-weighting relation[32].

The upshot of our simulations performed within the semi-grand canonical ensemble was to provide accurate numerical data, from which an equilibrium distribution function, $\mathcal{P}(T, \mu_\Delta; \varepsilon, x_\mathrm{s})$, could be derived for each given set of values of T and μ_Δ. With $\varepsilon = E/N$ representing the internal interaction energy per particle and x_s the sterol concentration, $\mathcal{P}(T, \mu_\Delta; \varepsilon, x_\mathrm{s})$ is proportional to the probability of finding the system in states characterized commonly by ε and x_s, and has the property, that if T and μ_Δ correspond to a point on a phase-coexistence boundary, then it will exhibit two degenerate local minima, representing the two coexisting phases. Thus, by analyzing the change in the 'landscape' of $\mathcal{P}(T, \mu_\Delta; \varepsilon, x_\mathrm{s})$ as values of T and μ_Δ are tuned, the phase boundary can be determined.

The umbrella sampling method was employed to this end and its implementation is described as follows. At values of T and μ_Δ estimated to be close to true coexistence conditions, a single but very long simulation is performed for a system of relatively small size L to yield an approximation of the equilibrium distribution function, $\mathcal{P}_L(T, \mu_\Delta; \varepsilon, x_\mathrm{s})$. When summed over x_s, $\mathcal{P}_L(T, \mu_\Delta; \varepsilon, x_\mathrm{s})$ yields the equilibrium distribution function $\mathcal{P}_L(T, \mu_\Delta; \varepsilon)$. A spectral free-energy function, defined by $\mathcal{F}_L(T, \mu_\Delta; \varepsilon) = -k_\mathrm{B}T \ln \mathcal{P}_L(T, \mu_\Delta; \varepsilon)$, displays a free-energy barrier between the two local minima. An iterative cycle is then set up:

1. Based on $\mathcal{F}_L(\varepsilon)$ an extrapolation based on the size dependence of the free energy barrier is used to approximate the barrier of a system of a larger size, L', and in turn, the following function:

$$f(T, \mu_\Delta; \varepsilon) = -\mathcal{F}_{L'}(T, \mu_\Delta; \varepsilon) = -\frac{L'}{L}\mathcal{F}_L(T, \mu_\Delta; \varepsilon) \ , \tag{10}$$

   when ε lies in the barrier region. $f(T, \mu_\Delta; \varepsilon)$, known as the shape function, defines the modified potential energy function as $\bar{H} = H + f(T, \mu_\Delta; \varepsilon)$.

2. $\bar{H}$ is used in a second simulation of a system of size L'. From this simulation, a modified probability distribution function, $\bar{\mathcal{P}}_{L'}(T, \mu_\Delta; \varepsilon, x_\mathrm{s})$, is obtained. The spectral free-energy function corresponding to the modified potential energy function should not show a significant barrier.

3. The required distribution function, $\mathcal{P}_{L'}(T, \mu_\Delta; \varepsilon, x_\mathrm{s})$, is easily reconstructed from $\bar{\mathcal{P}}_{L'}(T, \mu_\Delta; \varepsilon, x_\mathrm{s})$[32].

4. Based on $\mathcal{P}_{L'}(T, \mu_\Delta; \varepsilon, x_\mathrm{s})$, a method known as the Ferrenberg-Swendsen reweighting technique[33]. is applied in order to obtain a better estimate of the coexistence condition, T^* and μ_Δ^* and an improved approximation of $\mathcal{F}(T^*, \mu_\Delta^*; \varepsilon)$ at coexistence from $\mathcal{F}_{L'}(T^*, \mu_\Delta^*; \varepsilon)$.

5. If desired, another iteration is started from step (1) with $\mathcal{F}_{L'}(T^*, \mu^*_\Delta; \varepsilon)$, either to obtain an improved statistical sampling of $\mathcal{P}_{L'}(T^*, \mu^*_\Delta; \varepsilon, x_\mathrm{s})$ for the same system size or to simulate a larger system.

This method enables us to simulate systems of relatively large sizes. Repeated applications of the above procedures for systems with systematically varying sizes can yield a series of size-dependent $\mathcal{P}_L(T^*, \mu^*_\Delta; \varepsilon, x_\mathrm{s})$. A finite-size analysis of the series of data based on the method of Lee and Kosterlitz[34] can provide information on the specific nature of the corresponding transition.

Nevertheless, the method is still quite time consuming. In the iterations, the system size can only be increased in very small steps; the statistics required to obtain the initial estimate of the spectral free-energy function $\mathcal{F}$ as described in step (1) is already considerable, being typically of the order of $50 \cdot 10^6$ MCS per particle for a system of size $L = 10$.

3.3 Calculation of Physical Quantities

Given that a simulation based on the MC procedure described above does in fact generate an ensemble of microscopic states that are distributed in the configuration space according to the equilibrium distribution, the macroscopic thermal average of a microscopic physical quantity, $\mathcal{O}$, can be approximated by its average over the ensemble of states, $\{\Omega_n, n = 1, ..., N_\mathrm{state}\}$:

$$\langle \mathcal{O} \rangle = \frac{1}{N_\mathrm{state}} \sum_{n=1}^{N_\mathrm{state}} \mathcal{O}(\Omega_n) \; , \tag{11}$$

where N_state is the total number of microscopic states in the ensemble. It is important to note that the precise value of N_state required for Eq. (11) to be a good approximation for the true thermodynamic averages depends on the nature and size of the system as well as the specific physical observable under investigation.

In general, the macroscopic thermodynamic quantities that are of interest for the systems that we have studied are response functions such as specific heat and isothermal area compressibility as well as a macroscopic conformational order parameter characterizing the conformational ordering of the lipid chains. The response functions can be calculated directly from the simulation data by using the fluctuation-dissipation theorems:

$$\mathrm{C}_\Pi(T) = \frac{1}{N \mathrm{k_B} T^2} [\langle H^2 \rangle - (\langle H \rangle)^2] \; , \tag{12}$$

$$\mathrm{K}(T) = \frac{1}{\mathrm{k_B} T \langle A \rangle} [\langle A^2 \rangle - (\langle A \rangle)^2] \; , \tag{13}$$

where H is the potential-energy function defined in Eq. (1), $\mathrm{C}_\Pi(T)$ is the molecular specific heat at constant Π, and $\mathrm{K}(T)$ is the isothermal area compressibility. The average conformational order parameter of the lipid chains is calculated as

$$\phi = \frac{1}{2} \left(\left\langle \frac{\sum_{i=1}^{N} (\mathcal{L}_{io} - \mathcal{L}_{id})}{\sum_{i=1}^{N} (\mathcal{L}_{io} + \mathcal{L}_{id})} \right\rangle + 1 \right) \; . \tag{14}$$

In addition to the physical quantities mentioned above, the so-called structure factors, which provide information on the lateral organization of the constituent molecules in the

system, have also been calculated, based on the simulations performed within the canonical ensemble. Two of them are listed here, for which numerical data will be provided later:

$$S_{\mathrm{T}}(\boldsymbol{q}) = \frac{1}{N}\{\langle\rho_{\mathrm{T}}(\boldsymbol{q})\rho_{\mathrm{T}}(-\boldsymbol{q})\rangle - \langle\rho_{\mathrm{T}}(\boldsymbol{q})\rangle^2\delta_{\boldsymbol{q},\mathbf{0}}\} \ ,$$
$$S_{\mathrm{s}}(\boldsymbol{q}) = \frac{1}{N}\{\langle\rho_{\mathrm{s}}(\boldsymbol{q})\rho_{\mathrm{s}}(-\boldsymbol{q})\rangle - \langle\rho_{\mathrm{s}}(\boldsymbol{q})\rangle^2\delta_{\boldsymbol{q},\mathbf{0}}\} \ . \tag{15}$$

Here $\rho_{\mathrm{T}}(\boldsymbol{q})$ is the Fourier transform of the total density, $\rho_T(\boldsymbol{r}) \equiv \sum_i \delta(\boldsymbol{r} - \boldsymbol{r_i})$ and $\rho_{\mathrm{s}}(\boldsymbol{q})$ the Fourier transforms of the partial density of the sterol molecules, $\rho_{\mathrm{s}}(\boldsymbol{r}) \equiv \sum_i \delta(\boldsymbol{r} - \boldsymbol{r_i})\mathcal{L}_{\mathrm{S}i}$.

Finally, some simulations performed in the canonical ensemble were also used to derive the tracer diffusion coefficient D. According to the Einstein relation, the diffusion constant can be expressed as

$$D = \lim_{t\to\infty} \frac{1}{2dt}\langle|\boldsymbol{r}(t) - \boldsymbol{r}(0)|^2\rangle \ , \tag{16}$$

where $d = 2$ is the number of spatial dimensions of membranes, t is time, and the factor in the angular brackets is the mean-square displacement of the diffusing particle over time interval t. In practice, the simulation data $\langle|\boldsymbol{r}(t) - \boldsymbol{r}(0)|^2\rangle$ was plotted as a function of t and the plot displayed linearity for sufficiently large t. D was then determined from the slope of the linear part of the plot. Since the simulations were carried out using Monte Carlo methods, the time scales are meaningful only in a relative sense, as opposed to the absolute physical time scales in the system.

A practical remark on the simulations may be useful. In each simulation run, the system was equilibrated over a period of 200,000 MCS, and the various physical quantities were averaged over a period of 5-20·10^6 MCS.

4 Results

In this section we present a selection of the results of the Monte Carlo simulations, in terms of the equilibrium phase diagrams, collective conformational ordering of the lipid chains and structural characterizations of the lipid-sterol bilayer membranes. All the results in this section were obtained using the potential energy functions and the simulation methods presented in the previous section.

4.1 Phase Diagrams

4.1.1 Pure Lipid Bilayers

The phase diagram obtained from our simulation study for model lipid bilayers in the absence of cholesterol[20] is shown in Fig. 7. The phase diagram was calculated using the potential of Fig. 3a and is represented in terms of temperature and the parameter, V_0/J_0, which is a measure of the relative strength of the two square-well attractions. The point of key importance in this phase diagram is the appearance of two distinct regimes, separated by a triple point, of different types of macroscopic interplay between the translational and conformational degrees of freedom. All the phase lines represent first-order phase

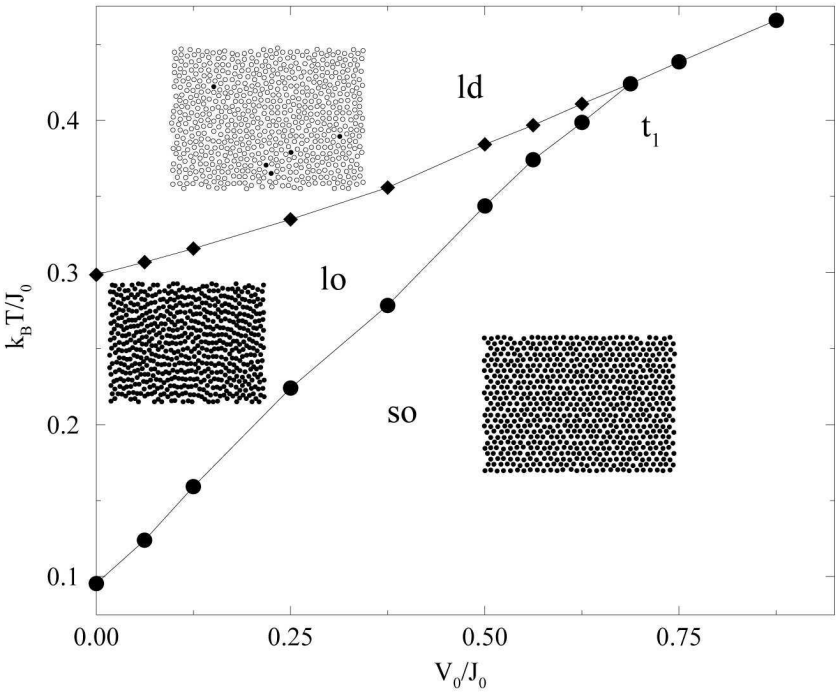

Figure 7. Phase diagram for the model of the pure lipid bilayer system. All three phase boundaries are first-order phase boundaries. The insets show snapshots of typical micro-configurations for the three different phases labeled **so** (solid-ordered), **ld** (liquid-disordered), and **lo** (liquid-ordered). Chains in the disordered state are plotted as (○) and chains in the ordered chain state as (●). The three snapshots are not given to scale. t_1 is the triple point described in the text.

transitions and a triple point is a phase point where two first-order phase lines join to form a single first-order phase line. The two degrees of freedom are uncoupled for values of V_0/J_0 smaller than the triple-point value, where two distinct ordering transitions from the **so** to the **lo** phases and from the **lo** to the **ld** phase take place successively. The first of these transitions is a solid-fluid transition where the conformational degrees of freedom do not change whereas the second transition is between two fluids where the conformation degrees of freedom change. However, the two degrees of freedom are macroscopically coupled for values of V_0/J_0 greater than the triple-point value and the intermediate **lo** phase vanishes. This is exactly the case of the main phase transition in single component lipid bilayers where one passes from directly from an **so** phase to an **lo** phase. We conclude, therefore, that although there is no fundamental reason why the intermediate **lo** phase cannot appear as a physical phase of a single-component lipid bilayer, the physical reality is such that the main phase transitions of single component lipid bilayers take place always above but close to the triple point. For our simulations for lipid-sterol systems, the values of the parameters in the model were then set such that the intermediate phase did not appear as a distinct thermodynamic phase of the corresponding system of pure lipid bilayers.

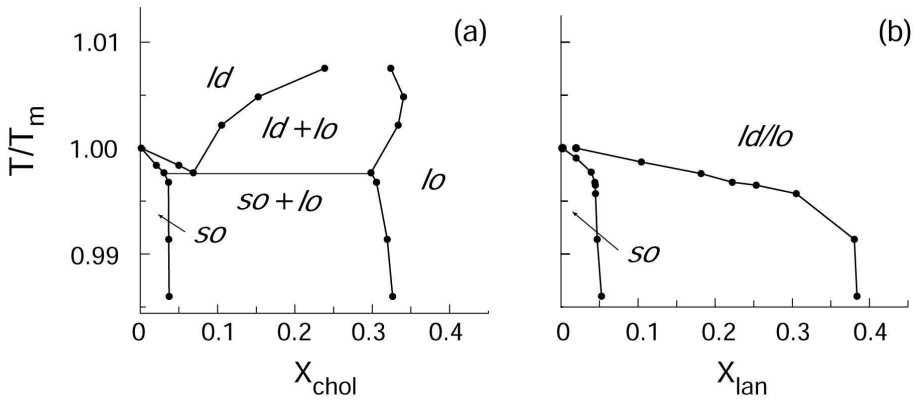

Figure 8. Theoretical phase diagrams determined from the Monte Carlo simulations of the microscopic model of interactions for the lipid-sterol membranes. (a) Lipid-cholesterol membranes; (b) lipid-lanosterol membranes.

4.1.2 Lipid-Sterol Bilayers

The simulated equilibrium phase diagrams for the lipid-cholesterol and the lipid-lanosterol membranes[21,22] are shown in Fig. 8. They were obtained from simulations in the semi-grand canonical ensemble and are presented in terms of the sterol concentration $x_{\rm s}$ (where $x_{\rm s}$= $x_{\rm chol}$ or $x_{\rm lan}$) and a reduced temperature, $T/T_{\rm m}$, where $T_{\rm m}$ is the main-transition temperature for the system of the pure lipid membrane. In terms of microscopic interaction parameters, the lipid-cholesterol systems are distinguished from the lipid-lanosterol systems by a rather modest (about 10 per cent) increase in the strength of the microscopic interactions between a sterol molecule and a lipid chain in its conformationally ordered state (see Table 1). This was illustrated in Fig. 3b.

It is clear from Fig. 8 that this small modification in the lipid-sterol interaction strength leads to considerable differences in the overall topologies of the two phase diagrams. In the case of lipid-cholesterol systems (Fig. 8a), the most significant characteristic of the phase diagram is a stable region of coexistence between the **ld** and **lo** phases. Associated with this coexistence are necessarily a stable critical point and the existence of a three-phase line. The critical point is found to be located close to $T \approx 1.0075T_{\rm m}$, $x_{\rm chol} \approx 0.298$ for the interaction parameters used in the simulations. The temperature of the three-phase coexistence is estimated to be $T = 0.9977T_{\rm m}$, and the concentrations of cholesterol in the three coexisting phases are $x_{\rm chol,so} = 0.030$, $x_{\rm chol,ld} = 0.068$, and $x_{\rm chol,lo} = 0.298$, respectively. By contrast, Fig. 8b shows that no **ld-lo** coexistence can be identified in the phase diagrams for the lipid-lanosterol systems. Correspondingly, only a metastable critical point exists and there is no three-phase line.

The systematic development of the stable **ld-lo** coexistence as lanosterol 'evolves' to cholesterol is a macroscopic signature of an increase in the capacity of the sterols to stabilize the **lo** phase. Another consistent signature is that with the sterol 'evolution,' the **lo** phase boundary of the low-temperature **so-lo** coexistence moves towards lower sterol concentrations, indicating a broadening of the region of stability of the **lo** phase in lipid-cholesterol bilayer membranes. A comparison between Fig. 2 and Fig. 8 shows a close correspondence between experimental and simulation results for both phase diagrams.

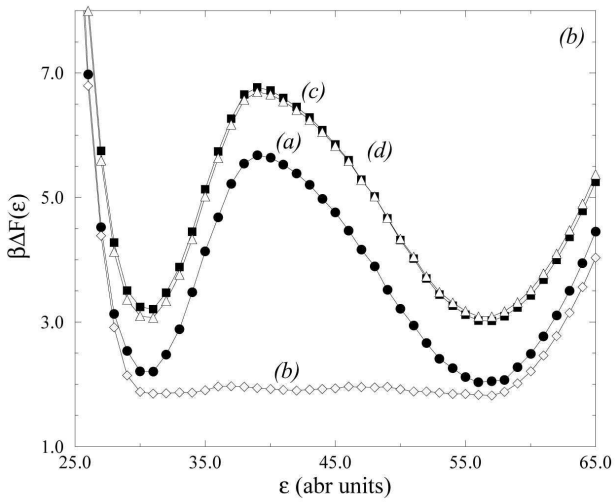

Figure 9. The different spectral free energies calculated using the modified potential-energy function. (a) The initial estimate of the shape function, $f(\varepsilon)$; (b) The spectral free-energy function for the modified potential-energy function; (c) The spectral free-energy function for the original system and (d) (open triangles) the spectral free-energy function at phase coexistence. $\beta = 1/k_B T$.

4.2 Umbrella Sampling and Finite-Size Analysis

It may be instructive at this point to demonstrate, with specific reference to the phase diagrams, how the umbrella sampling technique and finite-size analysis were used to determine the phase diagrams[21,29].

First, Fig. 9 shows the results from the different steps in the iteration procedure of the umbrella sampling described previously, which was applied in the simulations of the theoretical model for single-component lipid bilayers. In this particular example, the transition between the **so** and the **ld** phases was investigated. At $T = 0.969T_{\rm m}$, a temperature just slightly below the transition temperature, an initial estimate for the spectral shape function was made for a small system $L = 14$. This estimate is shown in curve (a) of the figure and has a distinct barrier between the two minima representing different phases. The shape function for a larger system, $L = 16$, was then obtained by the rescaling given in Eq. (10) and the spectral free energy for the modified potential-energy function was derived from the new simulation based on the modified energy function, as shown in curve (b). The spectral free energy corresponding to the original potential-energy function (shown in curve (c)) was reconstructed. Finally, use of the re-weighting technique yielded the spectral free energy at coexistence $T = T_{\rm m}$, now shown in curve (d).

Next, finite-size analysis was used to deal with the simulation data obtained for the two types of lipid-sterol systems in order to determine if phase coexistence occurred or not in the thermodynamic limit or if a critical point existed as a terminal point for the **ld–lo** coexistence. Figure 10 gives examples of such a finite-size analysis for the lipid-cholesterol system (refer to the phase diagram in Fig. 8a). This figure shows the spectral free energies, $\mathcal{F}_{\rm L}(x_{\rm s})$, calculated as a function of the system size L using umbrella sampling, for the **so–lo** coexistence at $T = 0.9860T_{\rm m}$ (Fig. 10a), the **ld–lo** coexistence at $T = 1.0035T_{\rm m}$

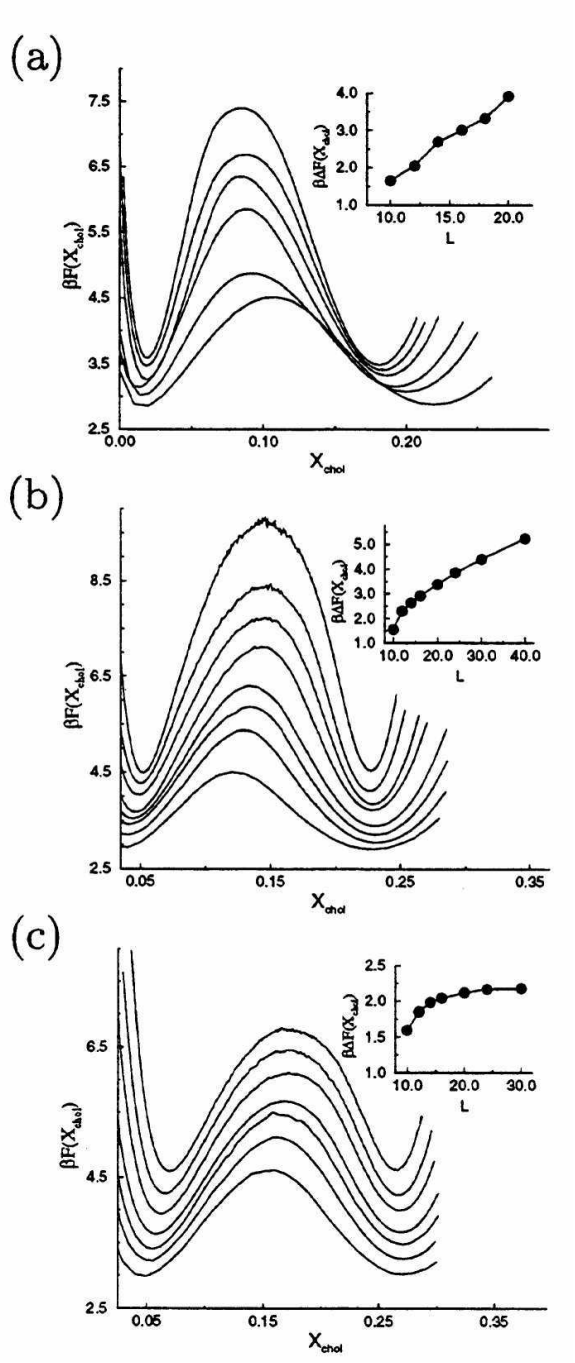

Figure 10. Finite-size scaling plots of both $\mathcal{F}_L(x_{\rm s})$ and the barrier height $\Delta\mathcal{F}_L(x_{\rm s})$ (the insets) at (a) $T = 0.9968T_{\rm m}$ (**so–lo** phase coexistence); (b) $T = 1.0035T_{\rm m}$ (**ld–lo** phase coexistence); (c) $T = 1.0075T_{\rm m}$ (close to the critical point). The system sizes are L= 8, 10, 12, 14, 16 and 20. $\beta = 1/k_BT$.

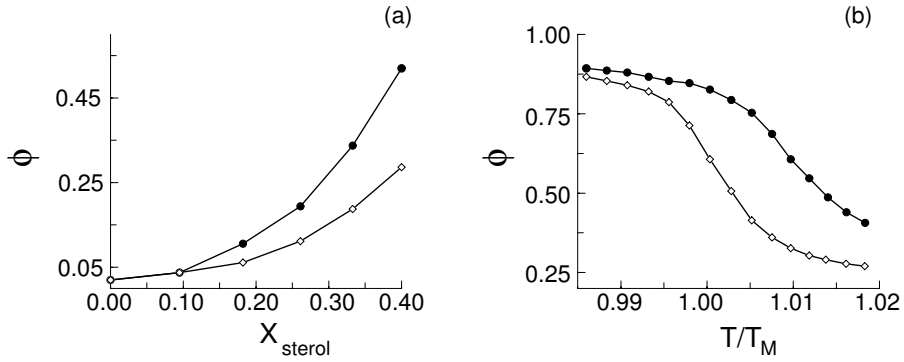

Figure 11. Theoretically calculated average of lipid-chain order parameter, ϕ, for the lipid-sterol membranes containing $N = 1600$ particles. The solid circles correspond to lipid-cholesterol membranes, and the open diamonds correspond to lipid-lanosterol membranes. (a) ϕ as a function of sterol concentration at a fixed temperature, $T = 1.0129T_{\rm m}$; (b) ϕ as a function of temperature for a fixed sterol concentration $x_{\rm s} = 0.367$.

(Fig. 10b), and the **ld–lo** coexistence at $T = 1.0075T_{\rm m}$. Shown in the insets are the corresponding barrier heights as a function of L for the three cases. In the first two cases, the barrier height increases linearly with L when L is sufficiently large. This finite-size behaviour is a characteristic of a first-order transition[34]. In the third case, however, the barrier height approaches a constant value as L is increased, indicating that $T = 1.0075T_{\rm m}$ is very close to the critical point terminating the the **ld–lo** coexistence.

4.3 Conformational Ordering of the Lipid Molecules

In order to characterize quantitatively the differential effects of the two sterols on the physical properties of lipid-sterol bilayer membranes[22], the calculated conformational order parameter, ϕ, as defined in Eq. (14), is presented in Fig. 11.

This thermal average represents the collective conformational ordering of the lipid molecules. Figure 11a shows ϕ as a function of sterol concentration for both types of the lipid-sterol systems at a fixed temperature $T = 1.0129T_{\rm m}$. This temperature is above that corresponding to the critical point of the **ld-lo** coexistence region of the lipid-cholesterol system. At this temperature, neither of the two types of the lipid-sterol systems undergo any phase transitions as the sterol concentration is changed. Figure 11b gives ϕ as a function of temperature for a fixed sterol concentration $x_{\rm s} = 0.367$. Clearly both cholesterol and lanosterol order the lipid chains, but the ordering effect of cholesterol is much stronger, qualitatively similar to what has been shown by the experimental data in Fig. 5. For example, Fig. 11a shows that cholesterol at $x_{\rm chol} = 0.40$ is able to rigidify close to 55 % of the lipid chains, whereas lanosterol at the same concentration can only rigidify roughly 30 %. This differential effect is also clearly illustrated in Fig. 12. Figure 12a and Fig. 12b are, respectively, snapshots of microscopic states of the lipid-cholesterol and the lipid-lanosterol systems in the **lo** phase.

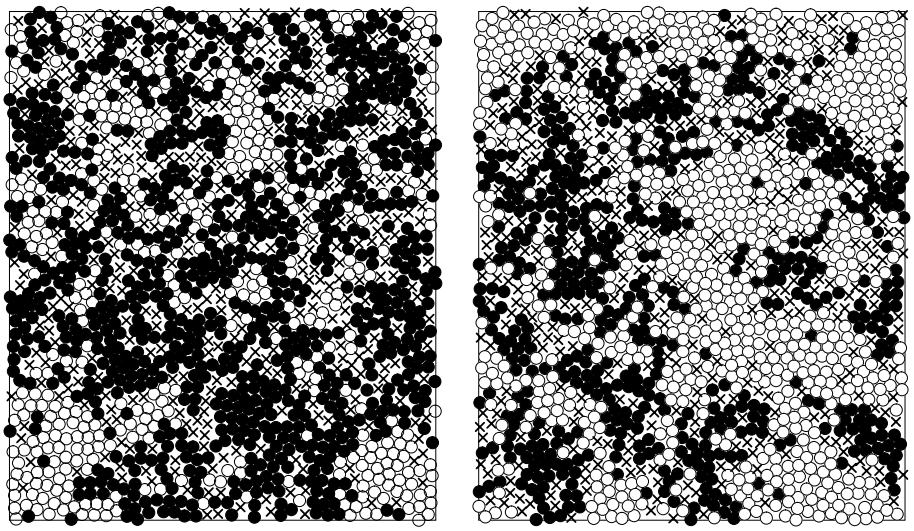

Figure 12. Snapshots of the micro-configurations for lipid-sterol systems in the **lo** phase very close to $T_{\rm m}$ when the sterol is cholesterol (the left-hand panel) and when the sterol is lanosterol (the right-hand panel). In the snapshots, a lipid chain in the ordered state is shown as (•), a lipid chain in the disordered state as (○) and a cholesterol molecule as (×).

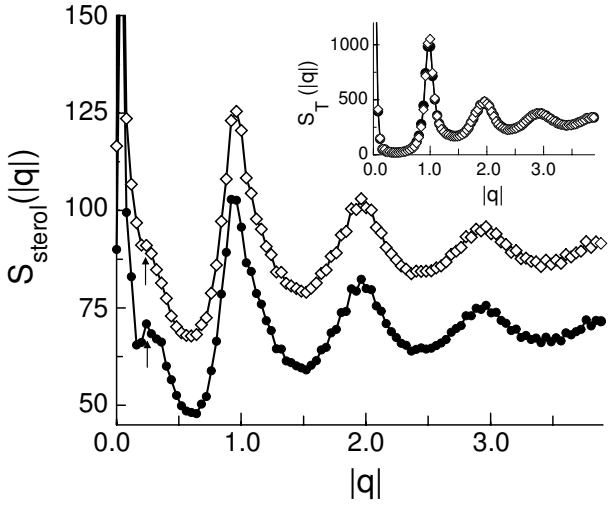

Figure 13. The partial structure factor describing the distribution of the sterol molecules in the membranes, $S_{\rm sterol}(|q|)$, calculated at $T = 0.9806T_{\rm m}$ and $x_{\rm s} = 0.367$. $S_{\rm chol}(|q|)$ is shown by the filled circles and $S_{\rm lan}(|q|)$ by the open diamonds. For clarity, the curve for $S_{\rm lan}(|q|)$ has been shifted along the y-axis. The values of $|q|$ are given in units of $2\pi/d$, where d is the hard-core diameter assigned to the particles. The arrows indicate an unusual structural signal in addition to the usual peaks characteristic of liquid structure. The inset shows the total structure factor, $S_{\rm T}(|q|)$, for the two lipid-sterol systems.

4.4 Molecular Organization

The MC simulations of the microscopic model allows us to analyze quantitatively the lateral distribution of the molecules in the lipid-sterol systems[21,22] in terms of the structure factors defined in Eq. (15). Figure 13 exhibits examples of the calculated structure factors calculated at $T = 0.9806T_{\rm m}$ and $x_{\rm s} = 0.367$, where the bilayers are in an **lo** state. The figure shows circular averages over the directions of the Fourier wave vectors, $\boldsymbol{q}$, of the sterol structure factor $S_{\rm sterol}(|\boldsymbol{q}|)$, characterizing the distributions of the sterol molecules. Shown in the inset are the circular averages of the total structure factor $S_{\rm T}(|\boldsymbol{q}|)$. The total structure factor has the typical features common to all liquid systems. The partial sterol structure factor, however, reveals more interesting structural information. Specifically, there appears a distinct, low-$|\boldsymbol{q}|$ peak at $|q| \simeq 0.35 \cdot 2\pi/d$, where d is the hard-core radius as discussed in the section describing the theoretical model. This particular q-value corresponds to a real-space length scale that covers several molecules, if a representative value of 5 Å for d may be used. The signal almost disappears in $S_{\rm lan}(|\boldsymbol{q}|)$ for the lipid-lanosterol systems.

4.5 Thread-Like Structures

Analysis of microscopic configurations such as those shown in Fig. 14 suggests that the special peak in the cholesterol structure factor is related to a micro-structure consisting of aligned 'threads'[22] of the cholesterol molecules, interspersed with 'threads' of lipid molecules with conformationally ordered chains as highlighted in Fig. 15. An qualitative analysis of the microscopic interactions in the model predicts that the stronger the interaction between a sterol molecule and an ordered lipid chain is, the more likely such micro-domains are to appear. This explains our observation through simulations that such micro-structures disappear almost entirely in the lipid-lanosterol systems, where the lipid-sterol interaction becomes weaker.

4.6 Lateral Diffusion

The simulation techniques used to monitor lateral diffusion in membranes were recently reviewed[35] and the differences between tracer diffusion and collective diffusion in relation to different types of experimental approaches were thoroughly discussed[36]. The lipid tracer diffusion coefficient in a model lipid-cholesterol binary mixture was calculated as a function of cholesterol concentration and temperature[37,36]. The model system that was studied was identical to that used in the calculation of the phase diagram of Fig. 8(a). The results are summarized in Fig. 16. The diffusion coefficient D increases monotonically with increasing temperature and this qualitative trend is independent of cholesterol concentration. The cholesterol concentration dependence of D, however, shows more interesting behaviour. At higher temperatures, D decreases with increasing $x_{\rm chol}$, while at temperatures below $T_{\rm m}$, D increases monotonically with $x_{\rm chol}$. At temperatures slightly greater than $T_{\rm m}$, D first decreases, then increases slightly with increasing $x_{\rm chol}$, as can be seen more clearly in the insert to the figure. A qualitative interpretation of the physical origin of this behavior is provided by the free volume theory of diffusion. An increase in D with $x_{\rm chol}$ is due to an increase in the free area per molecule with increasing $x_{\rm chol}$. Decreases in D arise from the fact that cholesterol also promotes conformational ordering of the lipid chains, which in turn causes the chains to interact more effectively, and

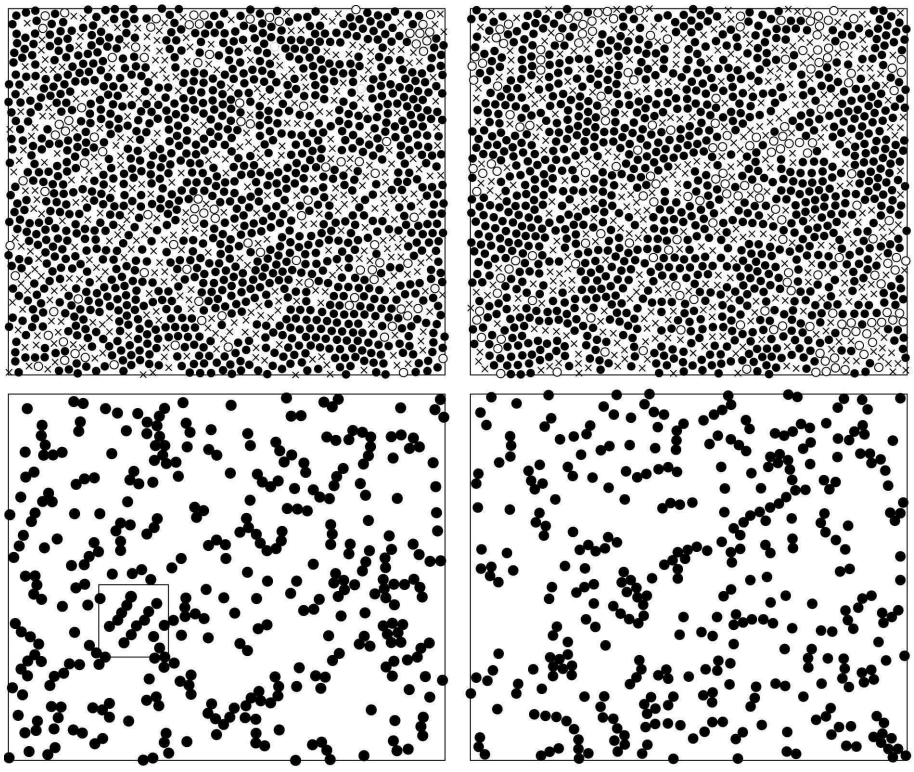

Figure 14. Snapshots of micro-configurations for lipid membrane systems containing cholesterol (left) and lanosterol (right), calculated at $T = 0.9806T_{\rm m}$ and $x_{\rm s} = 0.367$. The upper panel shows all particles, with lipid chains in the ordered state shown by filled circles, lipid chains in the disordered state shown by open circles, and sterol molecules shown by crosses. The lower panel shows only the corresponding sterol molecules as filled circles. The part highlighted by the box in the lower left snapshot is shown in detail in Fig. 15.

thus increase the effective activation energy for particle movement. These two effects compete with one another and give rise to the non-monotonic variation of D with $x_{\rm chol}$ at intermediate temperatures. The diffusion results of Fig. 16 are qualitatively consistent with those of a Fluorescence-Recovery-After-Photobleaching (FRAP) experimental study of lateral diffusion in dimyristoylphosphatidylcholine (DMPC)-cholesterol binary mixture model membranes[38]. Thus, the minimal model designed to reproduce the phase behaviour of lipid-sterol mixtures also yields a correct description of the equilibrium dynamics.

5 The Final Words

In this set of lecture notes we gave a detailed description of our minimal, off-lattice models for lipid-cholesterol and lipid-lanosterol bilayers using random-lattice simulation techniques. The difference in behavior between these two sterols was modeled, based on their specific molecular characteristics, in terms of their differential interactions with lipid molecules, namely, that cholesterol tends to rigidify neighboring lipid chains more strongly

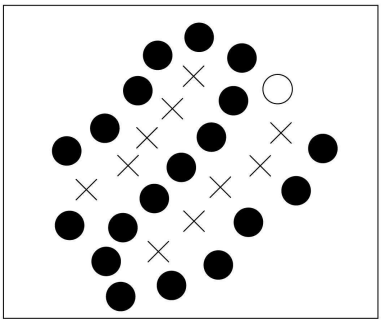

Figure 15. Enlarged version of the box highlighted in Fig. 14, showing a local 'thread-like' distribution of lipid and cholesterol molecules. Lipid chains in the ordered state are shown by filled circles, lipid chains in the disordered state are shown by open circles, and cholesterol molecules are shown by crosses.

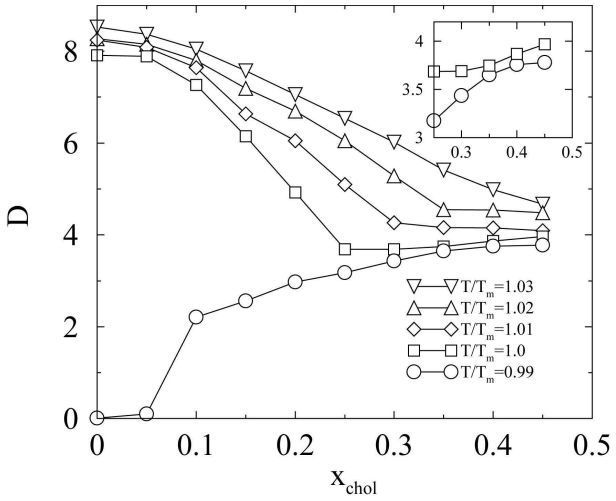

Figure 16. Diffusion coefficient D vs cholesterol concentration fraction $x_{\rm s}$. The inset shows the data for $T = 0.99T_{\rm m}$ and $1.0T_{\rm m}$ in an expanded scale to illustrate the increase in D with $x_{\rm chol}$ in the **lo** phase. The diffusion results for D are given in units of $d^2/{\rm MCS} \times 10^6$, where d is the hard-core diameter.

than lanosterol due to the relative smoothness of its α-face compared to that of lanosterol. We also discussed the MC method as well as the algorithm used in the MC simulations of the model. We also presented applications of various modern statistical-mechanical methods used to obtain the phase behavior of both lipid-cholesterol and lipid-lanosterol bilayers.

We were able to establish the occurrence/absence of the **lo** phase as a distinct, thermodynamically stable phase in the lipid-cholesterol and lipid-lanosterol system, respectively. We pointed out that this might have significant implications for understanding sterol evolution within the context of the structural evolution of membranes as well as the sterol requirement for the formation of rafts. In particular our results correlate with the current

hypothesis that cholesterol is an important factor in the formation of rafts and their stability and that lanosterol is unable to stabilize rafts.

We were also able to use our model to predict the behavior of the diffusion constant in lipid-cholesterol systems as a function of both temperature and cholesterol concentration. No additional parameters or parameter values were used in these simulations and the results were found to agree qualitatively with experimental results. It is significant that the minimal theoretical models have both descriptive and predictive capabilities, as this shows that the essential microscopic physical mechanisms have been included correctly in the models.

Acknowledgments

This work was supported by the Danish Natural Science Research Council, le FCAR du Quebec (Canada) via centre and team grants, and the NSERC of Canada via operating and equipment grants. MEMPHYS – Center for Biomembrane Physics is supported by the Danish National Research Foundation. Both MN and LM acknowledge support from the Danish Research Academy.

References

1. The present set of lecture notes is based on a recent review article by the present authors, M. J. Zuckermann, M. Bloom, J. H. Ipsen, L. Miao, O. G. Mouritsen, M. Nielsen, J. Polson, J. Thewalt, I. Vattulainen, and H. Zhu, Meth. Enzymol. (in press, 2003).
2. S. I. Singer and G. L. Nicolson, Science **175**, 720 (1972).
3. O. G. Mouritsen and O. S. Andersen (eds.). *In Search of a New Biomembrane Model*, Biol. Skr. Dan. Vid. Selsk. **49** (1998) 224.
4. K. Simons and E. Ikonen, Nature **387**, 569 (1997); D. Brown and E. London, J. Biol. Chem. **275**, 17221 (2000).
5. F. R. Maxfield, Curr. Opin. Cell Biol. **14**, 483 (2002).
6. U.Esmann and M. L. Berkowitz, Biophys. J. **76**, 2081 (1999).
7. P. B. Moore, C. F. Lopez, and M. K. Klein, Biophys. J. **81**, 2484 (2001).
8. H. L. Scott, Curr. Opin. Struct. Biol. **12**, 495 (2002).
9. L. Saiz, S. Bandyopadhyay, and M. L. Klein, Bioscience Rep. **22**, 151 (2002).
10. C. Hofsass, E. Lindahl, and O. Edholm, Biophys. J. **84**, 2192 (2003).
11. M. Patra, M. Karttunen, M. Hyvönen, E. Falck, P. Lindqvist, and I. Vattulainen, Biophys. J. **84**, 3636 (2003).
12. R. Böckmann, A. Hac, T. Heimburg, and H. Grubmüller, Biophys. J. **85**, 1647 (2002).
13. A. M. Smondyrev and M. L. Berkowitz, Biophys. J. **80**, 1649 (2001).
14. S. W. Chiu, E. Jakobsson, R. J. Mashl, and H. L. Scott, Biophys. J. **83**, 1842 (2002).
15. See for example: G. W. Feigenson and J. T. Buboltz, Biophys. J. **80**, 2775 (2001).
16. J. H. Ipsen, G. Karlström, O. G. Mouritsen, H. Wennerström, and M. J. Zuckermann, Biochim. Biophys. Acta **905**, 162 (1987); J. H. Ipsen, M. J. Zuckermann, and O. G. Mouritsen In *Cholesterol in Model Membranes* (L. X. Finegold, ed.) CRC Press, Boca Raton, Florida, 1993, pp. 223-257.

17. S. Doniach, J. Chem. Phys. **68**, 4912-4916 (1978).
18. O. G. Mouritsen, B. Dammann, H. C. Fogedby, J. H. Ipsen, C. Jeppersen, K. Jørgensen, J. Risbo, M. C. Sabra, M. M. Sperotto, and M. J. Zuckermann, Biophys. Chem. **55**, 55 (1995).
19. O. G. Mouritsen. In *Advances in the Computer Simulations of Liquid Crystals* (P. Pasini and C. Zannoni, eds.) Kluwer Academic Publ. Dordrecht, 2000, pp. 139-187.
20. M. Nielsen, L. Miao, J. H. Ipsen, O. G. Mouritsen, and M. J. Zuckermann, Phys. Rev. E **54**, 6889 (1996).
21. M. Nielsen, L. Miao, J. H. Ipsen, M. J. Zuckermann, and O. G. Mouritsen, Phys. Rev. E **59**, 5790 (1999).
22. L. Miao, M. Nielsen, J. Thewalt, J. H. Ipsen, M. Bloom, M. J. Zuckermann, and O. G. Mouritsen, Biophys. J. **82**, 1429 (2002).
23. M. C. Sabra and O. G. Mouritsen, Meth. Enzymol. **321**, 263 (2000).
24. M. Vist and J. H. Davis, Biochemistry **29**, 451 (1990).
25. J. Thewalt and M. Bloom, Biophys. J. **63**, 1176 (1992); J. Thewalt, F. M. Hanert, M. Liseisen, A. J. Farral, and M. Bloom, Pharmacology **42**, 9 (1992).
26. K. Bloch, Science **150**, 19 (1965); CRC Crit. Rev. Biochim. **14**, 47 (1983).
27. X. Xu and E. London, Biochemistry **39**, 843 (2000).
28. An excellent textbook for both MC and Molecular Dynamics is: D. Frenkel and B. Smit, *Understanding Molecular Dynamics*, 2nd Edition, Computational Science Series, Vol. 1, Academic Press, 2002.
29. M. Nielsen, Ph. D. Thesis, McGill University, Montreal, 1999.
30. S. Marcelja, Biochim. Biophys. Acta **367**, 165 (1974).
31. D. A. Pink, T. J. Green, and D. Chapman, Biochemistry **19**, 349 (1980).
32. J. Risbo, Ph. D. Thesis, Technical University of Denmark, 1997; J. Risbo, G. Besold, and O. G. Mouritsen, Comp. Mat. Sci. **15**, 311 (1999).
33. A. M. Ferrenberg and R. H. Swendsen, Phys. Rev. Lett. **61**, 2635 (1988); *ibid* **63**, 1195 (1991).
34. J. Lee and J. L. Kosterlitz, Phys. Rev. Lett. **65**, 137 (1990); Phys. Rev. B **43**, 3625 (1991).
35. I. Vattulainen and O. G. Mouritsen. In *Diffusion in Condensed Matter* (J. Kärger, P. Heitjans, and R. Haberlandt, eds.) Springer-Verlag, Berlin (in press, 2003).
36. I. Vattulainen, J. H. Ipsen, and O. G. Mouritsen, Biophys. J. (submitted, 2003).
37. J. M. Polson, I. Vattulainen, H. Zhu, and M. J. Zuckermann, Eur. Phys. J. **5**, 485 (2001).
38. P. F. F. Alameida, W. L. C. Vaz, and T. E. Thomson, Biochemistry **31**, 6739 (1992).